Simultaneous segmentation and distortion correction on diffusion weighted MR using shape priors

Oscar Esteban[1,2], Alessandro Daducci[2], Meritxell Bach-Cuadra[2,3], Jean-Philippe Thiran[2,3], Andrés Santos[1], and Dominique Zosso[2,4]

[1] Biomedical Image Technologies (BIT), ETSI Telecomunicación - Universidad Politécnica de Madrid and CIBER-BBN,
Av. Complutense 30, E-28040 Madrid, Spain
phd@oscaresteban.es,
[2] Signal Processing Laboratory (LTS5), École Polytechnique Fédérale de Lausanne (EPFL)
EPFL STI IEL LTS5, Station 11, CH-1015 Lausanne, Switzerland
[3] Dept. of Radiology, University Hospital Center (CHUV) and University of Lausanne (UNIL)
Rue du Bugnon 46, CH-1011 Lausanne, Switzerland
[4] Department of Mathematics, University of California, Los Angeles (UCLA)
520 Portola Plaza, Box 951555, Los Angeles, CA 90095-1555, USA

Abstract In whole-brain connectivity analysis of diffusion weighted MR images (DWI), an accurate delineation of the white-matter and grey-matter surfaces is required. While high-standard segmentation is readily available for anatomical MRI, such as T1-weighted, DWI typically have drastically lower resolution and severe geometrical distortions. We propose a DWI segmentation-registration framework that exploits the detailed anatomy extracted from anatomical MRI as shape-prior. We use an "active contours without edges"-like model to look for a deformation field that optimally maps the shape prior on the multivariate features in diffusion space. This joint approach reflects the intrinsic coupling of segmentation and distortion correction. Complementary, a precise and consistent cortical parcellation on DWI is straightforward by projection from T1 space. Thus, we expect to improve the reliability and robustness of the resulting connectivity networks and their comparability within and across subjects. Preliminary results on synthetic datasets and simulated DWI confirm the effectiveness of our approach.

Keywords: magnetic resonance, diffusion weighted imaging, distortion correction, segmentation, registration, shape priors, connectomics, echo planar imaging

1 Introduction

Diffusion Weighted Imaging (DWI) is a widely used family of Magnetic Resonance (MR) techniques [21] which recently has accounted for a growing interest in its application to whole-brain structural connectivity analysis. This emerging field, coined in 2005 as *MR Connectomics* [8, 20], currently includes a large amount of imaging techniques for acquisition, processing, and analysis specifically tuned for DWI data.

The whole-brain connectivity analysis has arisen some challenges that should be overcome in order to get reliable structural information about the neuronal tracts from

DWI [14, 15]. The earlier stages of these processing pipelines generally include two necessary steps, brain tissue segmentation on the diffusion space and the correction of geometrical distortions inherent to the imaging techniques [9].

In this work, we will refer as brain tissue segmentation to the precise delineation of the cerebrospinal fluid (CSF)-Grey Matter (GM) and GM-White Matter (WM) interface surfaces. This segmentation is an important step on which strongly rely further tasks. In tractography, a high-standard WM mask is required. Otherwise, there is an important risk for the algorithm to lose fiber bundles. This requirement is usually solved in practice by plainly thresholding the fractional anisotropy (FA), a well-know scalar map derived from DWI which depicts the isotropy of water diffusion inside the brain. Additionally, a precise location of the GM-WM surface is required in the final steps to achieve a consistent parcellisation of the cortex to represent the nodes of the output network. This parcellisation is generally defined in a high-resolution and better understood structural Magnetic Resonance Imaging (MRI) of the same subject (e.g. T1 and/or T2 weighted acquisitions). Conversely, this problem is resolved with non-linear registration of a structural MRI of the subject to the DWI data. Even though some efforts have addressed the study of the robustness of tractography versus the intra-subject variability [25, 10], the results produced are restricted to relevant regions of the brain. Therefore, extremely robust and precise segmentation methods are required in the whole-brain application.

On the other hand, the DWI data is usually obtained with echo-planar imaging (EPI) acquisition techniques, that often suffer from severe distortions due to local field inhomogeneities. Generally, it is appreciated in the anterior part of the brain, along the phase-encoded direction. Some methodologies have been developed and generically named as *EPI-unwarp* techniques [11, 12, 13, 19]. They usually require the extra acquisition of the magnitude and phase of the field (field-mapping), condition which is not always met. Some other methodologies do not make use the field-mapping, compensating the distortion with non-linear registration from structural MRI or other means [1]. To our knowledge, there exists no study of the impact of the EPI distortion on the variability of tractography results.

In this paper we propose a novel registration framework to simultaneously solve the segmentation and distortion challenges, by exploiting as strong shape-prior the detailed anatomy extracted from anatomical MRI. On one hand, the significant benefits of exploiting the anatomical MRI have been demonstrated [26], justifying the use of the shape prior information. On the other, the significant coupling between both problems demands for consistent segmentation, parcellation, and distortion. This need is satisfied by the use of a unique underlying model of our joint approach. We reformulate the segmentation problem as an inverse problem, where we seek for an underlying deformation field (the distortion) mapping from the structural space into the diffusion space.

2 Methods

2.1 Active Contours without edges-like variational segmentation model

Let us denote $\{c_i\}_{i=1..N_c}$ the nodes of a shape prior surface. In our application, a precise WM-GM interface extracted from a high-resolution reference volume. All the formulations can be naturally extended to include more shape priors. On the other hand, we have a number of DWI-derived features at each voxel of the volume. Let us denote by x the voxel and $f(x) = [f_1, f_2, \ldots, f_N]^T(x)$ its associated feature vector.
The transformation from reference into DWI coordinate space is achieved through a dense deformation field $u(x)$, such that:

$$c_i' = T\{c_i\} = c_i + u(c_i) \tag{1}$$

Since the nodes of the anatomical surfaces might lay off-grid, it is required to derive $u(x)$ from a discrete set of parameters $\{u_k\}_{k=1..K}$. Densification is achieved through a set of associated basis functions Ψ_k (e.g. rbf, interpolation splines):

$$u(x) = \sum_k \Psi_k(x) u_k \tag{2}$$

Consequently, the transformation writes

$$c_i' = T\{c_i\} = c_i + u(c_i) = c_i + \sum_k \Psi_k(c_i) u_k \tag{3}$$

Based on the current estimate of the distortion u, we can compute "expected samples" within the shape prior projected into the DWI. Thus, we now estimate region descriptors of the DWI features $f(x)$ of the regions defined by the priors in DWI space. Using Gaussian distributions as region descriptors, we propose an Active Contours without edges (ACWE)-like, piece-wise constant, variational image segmentation model (where the unknown is the deformation field) [4]:

$$E(u) = \sum_{\forall R} \int_{\Omega_R} (f - \mu_R)^T \Sigma_R^{-1} (f - \mu_R) dx \tag{4}$$

where R indexes the existing regions and the integral domains depend on the deformation field u. Note that minimizing this energy, $\text{argmin}_u\{E\}$, yields the maximum a posteriori (MAP) estimate of a piece-wise smooth image model affected by Gaussian additive noise. This inverse problem is ill-posed [2, 7]. In order to account for deformation field regularity and to render the problem well-posed, we include limiting and regularization terms into the energy functional [17, 22]:

$$\begin{aligned} E(u) = &\sum_{\forall R} \{ \int_{\Omega_R} (f - \mu_R)^T \Sigma_R^{-1} (f - \mu_R) dx \} \\ &+ \alpha \int \|u\|^2 dx + \beta \int \left(\|\nabla u_x\|^2 + \|\nabla u_y\|^2 + \|\nabla u_z\|^2 \right) dx \end{aligned} \tag{5}$$

These regularity terms ensure that the segmenting contours in DWI space are still close to their native shape. The model easily allows to incorporate inhomogeneous and

anisotropic regularization [18] to better regularize the EPI distortion.

At each iteration, we update the distortion along the steepest energy descent. This gradient descent step can be efficiently tackled by discretizing the time in a forward Euler scheme, and making the right hand side semi-implicit in the regularization terms:

$$\frac{u^{t+1}-u^t}{\tau} = -\sum_{i=1}^{N_c}\left[e(f(c_i'))\hat{n}_{c_i'}\Psi_{c_i}(x)\right] - \alpha u^{t+1} + \beta\Delta u^{t+1} \tag{6}$$

where the data terms remain functions of the current estimate u^t, thus $c_i' = c_i'(u^t)$. For simplicity on notation, we restricted the number of priors to only 1. We also defined $e(f(c_i')) = E_{out}(f(c_i')) - E_{in}(f(c_i'))$, and $E_R(f) = (f-\mu_R)^T\Sigma_R^{-1}(f-\mu_R)$. We applied a spectral approach to solve this implicit scheme:

$$u^{t+1} = \mathcal{F}^{-1}\left\{\frac{\mathcal{F}\{u^t/\tau - \sum_{i=1}^{N_c}\left[e(f(c_i'))\hat{n}_{c_i'}\Psi_{c_i}(x)\right]\}}{\mathcal{F}\{(1/\tau+\alpha)I - \beta\Delta\}}\right\} \tag{7}$$

3 Data and experiments

3.1 Shape prior

As described in section 1, the general situation in the connectivity pipelines consists of having a reliable segmentation obtained from the high resolution T1-weighted (T1) reference image. Therefore, a precise location of the tissue interfaces of interest is available in a reference space. Given that the anatomical reference segmentation is beyond the scope of this manuscript, we simply rely on the true contours known from the underlying models, and do not seek to establish them in a separate segmentation step on "anatomical" images.

3.2 Synthetic gray-scale data

The first, toy example is inspired by a problem shown for coupled CSF/GM and GM/WM segmentation in [16]. These authors note that "partial volume effects blur the distinction between closely adjacent surfaces in deep sulci, leading to a well-known segmentation error in which the deeper reaches of sulci are not penetrated by the putative surface model." This problem is aggravated in DWI, since the resolution tends to be worse compared to the anatomical images considered in [16]. They test their coupled segmentation algorithm on an image, "representing a sulcus in which the distinction between opposing banks of the sulcus has been obscured by partial volume."

Here, we have reproduced a very similar model. A volume consists of three piecewise-constant parts: a notched ball representing the white matter with a single sulcus ($\mu_{WM} = 0.8$), a cortical sheet of grey-matter obtained through dilation of the WM ($\mu_{GM} = 0.5$), and the surrounding background representing CSF ($\mu_{CSF} = 0.2$). The volume is then affected by additive Gaussian noise, effectively creating uniform standard deviation of $\sigma = 0.045$ per region.

As illustrated in Figure 1, conventional single surface segmentation of the CSF/GM boundary misses to capture the sulcus in its full depth. With our proposed model, we expect the joint segmentation-registration to be driven largely by the inner, GM/WM contour that exhibits sufficient contrast and lesser partial volume effects. The shape prior of the outer, difficult contour will then be co-aligned through the regularity of the estimated deformation field.

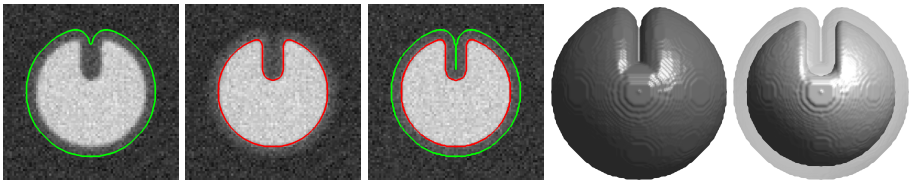

a) b) c) d) e)

Figure 1. The gray-scale sulcus model. a) The apparent CSF/GM boundary is affected by partial volume in the sulcal cavity, and conventional segmentation is likely to miss it. b) The GM/WM interface here has consistently good contrast. c) Registering the two shape priors coupled through deformation field regularity is expected to guide the CSF/GM contour. d&e) 3D view of the two shape priors.

3.3 Simulated diffusion data

In order to demonstrate the functionality of the methodology, and characterize its possibilities with diffusion data, we simulated the DW signal of a synthetic phantom from a model consisting of several spherical shapes emulating the different brain tissues (see Figure 2, first row). We reconstructed the signal with standard procedures to approximate the environment to the real one at maximum.

Signal simulation To numerically simulate the MRI signal attenuation when applying a diffusion gradient in a voxel with N fiber populations we made use of the standard *Multi-Tensor Model* [24]:

$$S(q)/S_0 = \sum_{i=1}^{N} f_i \exp\left(-b\, q^T \mathbf{D}_i\, q\right) + f_{iso} \exp\left(-b\, \mathbf{D}_{iso}\right), \tag{8}$$

where $q \in \mathbb{S}^2$ is the direction of the diffusion gradient applied, b is the b-value accounting for its strength, $S_0 \equiv S(0)$ is the signal with no diffusion weighting, f_i and $\mathbf{D}_i$ are respectively the volume fraction and the diffusion tensor characterizing the i-th fiber population.

The diffusion tensors $\mathbf{D}_i$ and $\mathbf{D}_{iso}$ describe the diffusion processes of each fiber compartment and of contaminations from the CSF. In this work, these quantities have been taken from standard ranges typically observed in the human brain [3].

Noise simulation The diffusion MRI signal S has been corrupted with *Rician noise* [6] as follows:

$$\tilde{S} = \sqrt{(S+\varepsilon_1)^2+\varepsilon_2^2} \tag{9}$$

where $\varepsilon_{1,2}$ are Gaussian distributed with zero mean and standard deviation $\sigma = S_0/SNR$ and SNR is the signal-to-noise ratio (SNR) on the S_0 image.

Derived scalar features The target DWI data is characterized by its distortions and its low resolution (typically around $2.2x2.2x3mm^3$). Depending on the posterior reconstruction methodology and the angular resolution intended, the DWI raw data has to be processed in order to extract the information in a manageable manner. The properties of the reconstructed tensors and derived scalar maps have been studied by [5]. Based on their findings, the proposed energy model adapts to the FA (10) and mean diffusivity (MD) (11) for their properties. Whereas FA describes the *shape* of diffusion, the MD depicts the *magnitude* of the process.

$$\mathrm{FA} = \sqrt{\frac{1}{2}}\frac{\sqrt{(\lambda_1-\lambda_2)^2+(\lambda_2-\lambda_3)^2+(\lambda_3-\lambda_1)^2}}{\sqrt{{\lambda_1}^2+{\lambda_2}^2+{\lambda_3}^2}} \tag{10}$$

$$\mathrm{MD} = (\lambda_1+\lambda_2+\lambda_3)/3 \tag{11}$$

There exist two main reasons to justify their choice. First, they are well-understood and standardized in clinical routine. Second, together they contain most of the information that is usually extracted from the DWI-derived scalar maps.

Simulated distortions For this model, we created manually a sound distortion visually similar to real EPI distortions. We interpolated the distortion to a dense deformation field, necessary for warping the raw DWI simulated data. Once the signal was deformed, we proceeded to reconstruct the Diffusion Tensor Imaging (DTI) and subsequently obtained the scalars of interest (FA, MD). Finally, we estimated their parameters using the tissue probability distribution maps from the original model (Table 1).

	μ_{FA}	μ_{MD}	Σ
WM	0.778	6.94×10^{-4}	$\begin{pmatrix} 4.85\times10^{-3} & -6.90\times10^{-6} \\ -6.90\times10^{-6} & 1.03\times10^{-8} \end{pmatrix}$
GM	0.119	8.95×10^{-4}	$\begin{pmatrix} 5.90\times10^{-4} & -1.43\times10^{-6} \\ -1.43\times10^{-6} & 1.04\times10^{-8} \end{pmatrix}$
CSF	0.103	2.99×10^{-3}	$\begin{pmatrix} 1.19\times10^{-3} & 2.22\times10^{-7} \\ 2.22\times10^{-7} & 1.56\times10^{-8} \end{pmatrix}$

Table 1. Model parameters

4 Results and discussion

4.1 Synthetic gray-scale data

4.2 Simulated diffusion data

The proposed method successfully reverted the synthetic distortion field we applied to the data. With 16x16x16 control points, the displacements field is dense enough to correctly represent the synthetic field. (INCLUDE FIGURE). Figure XX shows the restored image and a difference map with the original model (we can also compute Dice indexes and that stuff).

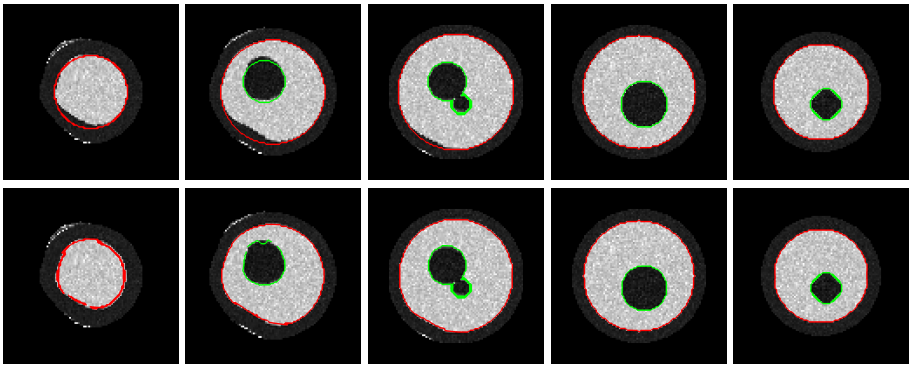

Figure 2. First row presents several slices along Z axis of the distorted FA map and the undistorted WM-GM and WM-CSF contours given as shape priors. Second row contains the same map, now with the contours after joint segmentation-registration.

5 Conclusions and outlook

A novel application for the ACWE framework is proposed, with the aim at recovering the displacement field underlying the EPI geometrical distortions. Exploiting the segmentation properties of the ACWE and optimizing the displacement field, we describe a registration-segmentation methodology that simultaneously segmented and restored the distortion on DWI-like synthetic data. Visual results and quantitative results are provided.

Once proven the aptness of the methodology to the application with simplistic synthetic data, in further studies we will cover the actual performance on real images and the benefits of overcoming the described challenges (segmentation and EPI distortion correction) in one single step.

We conclude stressing on the importance of tackling with the numerous challenges that exist on the DWI data processing in order to achieve reliable results on the whole-brain connectivity analysis.

Bibliography

[1] Andersson, J.L.R., Hutton, C., Ashburner, J., Turner, R., Friston, K.: Modeling geometric deformations in EPI time series. Neuroimage 13(5), 903–919 (2001), http://www.sciencedirect.com/science/article/pii/S1053811901907463

[2] Bertero, M., Poggio, T.A., Torre, V.: Ill-posed problems in early vision. In: Proceedings of the IEEE. vol. 76, p. 869–889 (1988)

[3] Canales-Rodríguez, E., Melie-García, L., Iturria-Medina, Y.: Mathematical description of q-space in spherical coordinates: Exact Q-ball imaging. Magn. Reson. Med. 61(6), 1350–1367 (2009)

[4] Chan, T.F., Vese, L.A.: Active contours without edges. IEEE Transactions on Image Processing 10(2), 266–277 (2001)

[5] Ennis, D.B., Kindlmann, G.: Orthogonal tensor invariants and the analysis of diffusion tensor magnetic resonance images. Magnetic Resonance in Medicine 55(1), 136–146 (2006), http://onlinelibrary.wiley.com/doi/10.1002/mrm.20741/abstract

[6] Gudbjartsson, H., Patz, S.: The Rician distribution of noisy MRI data. Magn. Reson. Med. 34(6), 910–914 (1995)

[7] Hadamard, J.: Sur les problèmes aux dérivées partielles et leur signification physique. Princeton University Bulletin 13, 49–52 (1902)

[8] Hagmann, P.: From diffusion MRI to brain connectomics. Ph.D. thesis, Institut de traitement des signaux PROGRAMME DOCTORAL EN INFORMATIQUE ET COMMUNICATIONS POUR L'OBTENTION DU GRADE DE DOCTEUR ÈS SCIENCES PAR Docteur en médecine, Université de Lausanne (2005), http://biblion.epfl.ch/EPFL/theses/2005/3230/EPFL_TH3230.pdf

[9] Hagmann, P., Grant, P.E., Fair, D.A.: MR connectomics: a conceptual framework for studying the developing brain. Frontiers in Systems Neuroscience 6 (Jun 2012), http://www.ncbi.nlm.nih.gov/pmc/articles/PMC3374479/, PMID: 22707934 PMCID: PMC3374479

[10] Heiervang, E., Behrens, T., Mackay, C., Robson, M., Johansen-Berg, H.: Between session reproducibility and between subject variability of diffusion MR and tractography measures. NeuroImage 33(3), 867–877 (Nov 2006), http://www.sciencedirect.com/science/article/pii/S1053811906008081

[11] Holland, D., Kuperman, J.M., Dale, A.M.: Efficient correction of inhomogeneous static magnetic field-induced distortion in echo planar imaging. NeuroImage 50(1), 175 (Mar 2010), http://www.ncbi.nlm.nih.gov/pmc/articles/PMC2819607/, PMID: 19944768 PMCID: PMC2819607

[12] Hsu, Y.C., Hsu, C.H., Tseng, W.Y.: Correction for susceptibility-induced distortion in echo-planar imaging using field maps and model-based point spread function. IEEE Transactions on Medical Imaging 28(11), 1850 –1857 (Nov 2009)

[13] Jezzard, P., Barnett, A.S., Pierpaoli, C.: Characterization of and correction for eddy current artifacts in echo planar diffusion imaging. Magnetic resonance

in medicine 39(5), 801–812 (2005), http://onlinelibrary.wiley.com/doi/10.1002/mrm.1910390518/abstract
[14] Johansen-Berg, H., Rushworth, M.F.: Using diffusion imaging to study human connectional anatomy. Annual Review of Neuroscience 32(1), 75–94 (2009), http://www.annualreviews.org/doi/abs/10.1146/annurev.neuro.051508.135735, PMID: 19400718
[15] Jones, D.K., Knösche, T.R., Turner, R.: White matter integrity, fiber count, and other fallacies: The do's and don'ts of diffusion MRI. NeuroImage (Jul 2012), PMID: 22846632
[16] MacDonald, D., Kabani, N., Avis, D., Evans, A.C.: Automated 3-d extraction of inner and outer surfaces of cerebral cortex from MRI. NeuroImage 12(3), 340–356 (2000), http://citeseerx.ist.psu.edu/viewdoc/download?doi=10.1.1.73.8698&rep=rep1&type=pdf
[17] Morozov, V.A.: Linear and nonlinear ill-posed problems. Journal of Mathematical Sciences II(6), 706–736 (1975)
[18] Nagel, H.H., Enkelmann, W.: An investigation of smoothness constraints for the estimation of displacement vector fields from image sequences. IEEE Transactions on Pattern Analysis and Machine Intelligence PAMI-8(5), 565–593 (Sep 1986), http://ieeexplore.ieee.org/lpdocs/epic03/wrapper.htm?arnumber=4767833
[19] Reber, P.J., Wong, E.C., Buxton, R.B., Frank, L.R.: Correction of off resonance-related distortion in echo-planar imaging using EPI-based field maps. Magnetic Resonance in Medicine 39(2), 328–330 (2005), http://onlinelibrary.wiley.com/doi/10.1002/mrm.1910390223/abstract
[20] Sporns, O., Tononi, G., Kötter, R.: The human connectome: A structural description of the human brain. PLoS computational biology 1(4), e42 (Sep 2005), PMID: 16201007
[21] Sundgren, P.C., Dong, Q., Gómez-Hassan, D., Mukherji, S.K., Maly, P., Welsh, R.: Diffusion tensor imaging of the brain: review of clinical applications. Neuroradiology 46, 339–350 (May 2004), http://www.springerlink.com/content/fa30k4q3h9kg4yjq/
[22] Tichonov, A.N.: Solution of incorrectly formulated problems and the regularization method. Soviet Mathematics 4, 1035–1038 (1963)
[23] Tuch, D.S.: Q-ball imaging. Magnetic Resonance in Medicine 52(6), 1358–1372 (2004), http://onlinelibrary.wiley.com/doi/10.1002/mrm.20279/full
[24] Tuch, D., Reese, T., Wiegell, M., Makris, N., Belliveau, J., Wedeen, V.: High angular resolution diffusion imaging reveals intravoxel white matter fiber heterogeneity. Magn. Reson. Med. 48(4), 577–582 (2002)
[25] Wakana, S., Caprihan, A., Panzenboeck, M.M., Fallon, J.H., Perry, M., Gollub, R.L., Hua, K., Zhang, J., Jiang, H., Dubey, P., Blitz, A., van Zijl, P., Mori, S.: Reproducibility of quantitative tractography methods applied to cerebral white matter. NeuroImage 36(3), 630–644 (Jul 2007), http://www.sciencedirect.com/science/article/pii/S1053811907001383
[26] Zöllei, L., Stevens, A., Huber, K., Kakunoori, S., Fischl, B.: Improved tractography alignment using combined volumetric and surface registration. NeuroImage 51(1), 206–213 (May 2010), http://www.sciencedirect.com/science/article/pii/S1053811910001400